Energy & Buildings 251 (2021) 111342

Contents lists available at ScienceDirect

Energy & Buildings

journal homepage: www.elsevier.com/locate/enb

Evaluating dynamic thermal performance of building envelope components using small-scale calibrated hot box tests

Zhenglai Shen [a], Adam L. Brooks [a], Yawen He [a], Som S. Shrestha [b], Hongyu Zhou [a,*]

[a] Department of Civil and Environmental Engineering, University of Tennessee at Knoxville, Knoxville, TN, USA
[b] Buildings and Transportation Science Division, Oak Ridge National Laboratory, Oak Ridge, TN, USA

ARTICLE INFO

Article history:
Received 24 March 2021
Revised 16 July 2021
Accepted 9 August 2021
Available online 12 August 2021

Keywords:
Calibrated hot box test
Scaled-down specimen
Dynamic thermal performance

ABSTRACT

The hot box test method has been applied to evaluate both the steady-state (U-value) and dynamic thermal properties of building envelopes. However, the high construction cost of full-scale hot box apparatus and the testing time required (usually several days) may prevent its wider adoption. To overcome the limitations of full-scale hot box tests, this paper proposes a novel method to evaluate the dynamic thermal performance of building envelope components using a small-scale calibrated hot box and scaled-down specimen. In this paper, the scaling relationships of thermal properties evaluated using a full-size specimen and a scaled-down specimen are established based on the Laplace transform of the heat transfer equations. In addition, dynamic thermal properties obtained from scaled-down experimental tests are compared to the values calculated by the EN ISO13768 (ISO) method. A small-scale hot box with a 355 mm × 355 mm metering area was constructed and calibrated to validate the correlations. Three scaled-down concrete sandwich wall panels were then tested and the scaling relationship was cross-validated using the experimental results, finite difference (FD) simulations, and the ISO method. The results indicate that the dynamic thermal properties obtained from a scaled-down hot box test can be correlated to its full-size counterpart when certain conditions are met. The scaled-down hot box test is demonstrated to be an effective yet economical alternative to a full-scale test with significantly reduced experimentation cost and turn-around time.

1. Introduction

The building sector is estimated to account for more than one-third of the total energy consumption worldwide [1], where a substantial portion is operational energy used for space heating and cooling [2]. In particular, the thermal exchange through opaque envelopes contribute more than 7% of primary energy consumption in the US [3]. Traditionally, the thermal performance of building components is often characterized by their thermal transmittance (i.e., U-value). Under steady-state conditions, U-value serves as a good indicator of the relative heat flux for building envelopes [4]. U-value based prescriptions are used by the current building codes such as ASHRAE 90.1, 90.2, and IECC to guide building envelope design. However, buildings are rarely in steady-state conditions due to the diurnal outdoor air temperature fluctuation and fluctuations in indoor temperature. For building envelopes, especially thermally massive building envelopes (e.g., concrete sandwich wall panel), the time and temperature amplitude reduction of diurnal outdoor air temperature fluctuation that penetrates through it is related to its U-value and its thermal mass [5]. Thus, the abstraction of conductivity values must be considered alongside other parameters. For example, the reduction of building operational energy requires a correct evaluation of the dynamic characteristics of opaque envelope components considering actual boundary conditions [6]. In addition, building design practice has introduced new design strategies based on the dynamic behavior of the building envelopes to improve its energy efficiency and the occupants' comfort [7]. Therefore, dynamic thermal performance is a critical consideration in building envelope design and evaluation.

The dynamic thermal performance of a building envelope components, such as a wall assembly, is characterized by parameters that identify its behavior when subjected to transient thermal loadings that are variable in time. Analytically, the European standard EN ISO 13,786 [8] describes the thermal exchange in a steady periodic regime between the indoor environment and the outdoor environment employing a matrix formulation. Such formulation allows for calculating the periodic thermal transmittance to

* Corresponding author at: 851 Neyland Drive, 417 John D. Tickle Building, Knoxville, TN 37996-2313, USA.
E-mail address: hzhou8@utk.edu (H. Zhou).

https://doi.org/10.1016/j.enbuild.2021.111342
0378-7788/

Nomenclature

A	Area
Amp	Amplitude
a, b, c, d	Coefficients of the finite difference discretization of 1D heat transfer equation [-]
a_1, b_1	Parameters related to the surface condition and materials
C_1, C_2	Constants (determined by boundary condition) [-]
c_p	Specific heat [J/kgK]
EXP	Experiment
el	Metering chamber interior edge length where walls meet
FD	Finite difference method
FS	Full size
f	Decrement factor [-]
h	Heat convection coefficient [W/m^{2}K]
$ISO\ method$	EN ISO 13768 method
j	Imaginary unit
L	Length along thickness of the envelope assembly [m]
m	Total nodes [-]
N	Total layers of a wall assembly [-]
n	Scaling-down coefficient of envelope assembly [-]
Q	Heat flow rate (W)
q	Heat flux [W/m^2]
$\bar{q}$	Laplace transform of heat flux
$\hat{q}$	Amplitude of heat flux [W/m^2]
R	Thermal resistance [m^{2}K/W]
s	Complex variable [-]
T	Temperature [K or ^{o}C]
$\bar{T}$	Laplace transform of temperature
$\hat{T}$	Amplitude of temperature
t	Time [s]
t_{lag}	Time lag [h]
U_0	Thermal transmittance coefficient
x	Length along x-axis [m]
Y_{12}	Periodic thermal transmittance
$\mathbf{Z}$	Heat transfer matrix
Z	Element of heat transfer matrix
Δt	Time increment of finite difference method [s]
$\Delta T_{ai\text{-}ao}$	Air to air temperature difference between inside and outside [^{o}C]
Δx	Distance increment of finite difference method [m]

Greek Symbols

α	Thermal diffusivity [m^2/s]
δ	Discretized distance between two continuous nodes of finite difference method [m]
ξ	Ratio of the thickness of the layer to the penetration depth [-]
ρ	Density [kg/m^3]
τ	Real part of a complex variable [-]
χ	Thermal conductivity [W/mK]
ψ	Complex variable of the ratio of the thickness of the layer to the penetration depth
ω	Imaginary part of a complex variable (angular frequency) [1/s]

Subscripts and superscripts

1	Outdoor surface
2	Indoor surface
ai	Indoor air
ao	Outdoor air
$cold$	Code side surface of the test specimen
eff	Effective property
ff	Frame and foam
fl	flanking of hot-side box
$frame$	Frame of the hot-side box
$foam$	Foam of the hot-side box
hot	Hot side surface of the test specimen
i	Node i located at location x_i of a finite difference discretization
ISO	EN ISO 13768
$input$	Input heat flow from power source
k	k-th layer of a N-layer wall assembly
$loss$	Heat flow loss due to metering wall, flanking, and frame and
mw	Metering wall of hot-side box
old	Node temperature at the previous step
$overall$	Overall property of a N-layer wall assembly
p	Number of metering chamber interior edges
SD	Scaled-down
si	Indoor surface
so	Outdoor surface
sp	Specimen

evaluate dynamic thermal properties such as the time lag and decrement factor. Gasparella et al. [9] applied both the EN ISO 13768 method (ISO method) and finite difference (FD) simulation to estimate opaque building envelope's dynamic thermal transfer properties under summer outdoor conditions. In their research, a correction factor was proposed to adjust the dynamic thermal properties calculated by the ISO method for forcing temperature profiles that are not harmonic. Rossi and Rocco [10] further studied the role of periodic thermal transmittance and internal areal heat capacity of the exterior wall design using the ISO method. Using finite-difference simulations, Asan [11] found that the thickness and type of the envelope material were two critical factors influencing the time lag and decrement factor. Furthermore, Al-Sanea et al. [12,13] studied the effects of thermal mass and insulation layer distribution. Ozel and Ozel [14] investigated the effect of wall orientation on time lag and the decrement factor. Balaji et al. [15] studied the effects of the thermal conductivity, thermal capacity, and thickness of the wall on time lag, decrement factor, and the corresponding heat flux variation and temperature distributions across wall sections.

Experimentally, the hot box test method has been applied to evaluate the dynamic thermal performance of building envelope components at full scale. During a hot box test, the specimen is positioned between two chambers, i.e., the metering chamber and the climate chamber, which simulate the interior environment (hot side) and the exterior environment (cold side), respectively. Heating and cooling systems are usually used in the metering chamber and climate chamber, respectively, to create steady or periodic temperature differences. There are two typical hot box setups, i.e., the guarded hot box and the calibrated hot box. For the guarded hot box setup, it uses a metering chamber inside a guard chamber. The guarded hot box keeps the guard chamber and the metering chamber close to the same temperature, and thus the heat loss through the metering box wall is minimized [16]. While the calibrated hot box uses the surrounding environment as the guard chamber by measuring the heat loss through the metering walls. So far, the hot box test has been used to evaluate both the static and dynamic thermal properties of building envelope components. Works related to using the hot box to measure the static thermal properties of building envelope components

(e.g., thermal transmittance) can be found in the recent review paper of Soares et al. [17]. With respect to using the hot box method to measure the dynamic thermal properties of building envelope components, Brown and Stephenson [18,19] presented one of the first methodologies for measuring the dynamic thermal properties of homogenous specimens using a guarded hot box, where seven wall specimens were experimentally tested under sinusoidal excitation in the cold chamber. The results showed good agreement between the measured and the predicted response factors. Ulgen [20] investigated ten different walls by using a hot box apparatus under sinusoidal excitation for a period of 24 h. Sala et al. [21] studied a hollow brick wall construction excited by a triangle forcing signal applied to the cold room. Martin et al. [22,23] further studied the method to calculate the response factor of a multi-layer wall with unknown material properties. They analyzed the effect of the thermal bridge on the heat flux amplitude and time lag. The results highlighted the importance of dynamic thermal tests on correctly estimating the building envelope's thermal properties. More recently, Bishara et al. [24] assessed the effect of uncertainties (boundary conditions, humidity, homogeneity of the forcing signal) on the building envelope's dynamic thermal properties.

All the above-mentioned studies use full-scale test specimens, which require large-scale test facilities, expensive construction of full-size specimens, and extensive instrumentations [25,26]. While full-scale hot box tests are demonstrated to provide reliable results, their high facility requirements and high costs prevent fast-turn-around experimentation and the trial-and-error process that may be involved in new material development or envelop design concept innovations. In addition, full-scale hot box tests are time-consuming since each sinusoidal cycle usually takes 24 h each cycle to mimic the environment temperature change for full-size specimens. Typically, several test cycles are needed to reach a steady periodic response. Therefore, there is a need to study the feasibility of using scaled-down specimens for both steady-state and dynamic thermal properties tests, which can be tested by relatively lower cost small-scale hot box apparatus with less testing time. To date, some preliminary studies have been conducted to develop small-scale (or reduced-scale) hot box for measuring the steady-state thermal properties of building envelope components (i.e., thermal conductivity and U-value) [27–31], where Seitz and MacDougall [27] and O'Leary and Duffy [30] emphasized the importance of designing affordable hot box testing apparatus due to the high cost of accredited laboratory and long waiting time. In the study by Seitz and MacDougall [27], a small-scale calibrated hot box apparatus was developed with a testing area of 1.18 m × 1.37 m (Width × Height). O'Leary and Duffy [30] constructed a small-scale hot box apparatus with a maximum specimen size of 0.715 m × 0.715 m. Modi et al. [29] designed a mini-scale hot box for measuring the U-value of an insulation building block prototype, where the hot box and the and cold box were built in the same large box, which was separated by the test specimen with sizes of 0.4 m × 0.2 m. More recently, Zhao et al. develop a small-scale hot box for characterizing the thermal properties of window insulation materials. Transparent aerogel specimens with the diameter of 0.2 m were tested where a heat flow meter was used to directly measure the heat flux penetrate through the specimen [25].

Despite the wide recognition of the needs to develop scaled-down hot box tests for cost-saving and faster experimental turn-around, there has not been any systematic study to draw the correlations between the dynamic thermal properties (e.g., time-lag and decrement factors) tested from scaled-down building envelope specimens with the performance of their full-scale counterparts. In addition, all existing research conducted to date has used small-scale hot box for steady-state evaluation (e.g., for determining R-value or U-value), whereas no attempt has been made to characterize the dynamic thermal behavior of building envelope using scaled-down specimens. Due to the scaling effect, the thermal response of a scaled-down specimen is different than that of a full-scale envelope assembly. Thus, without elucidating the relationships linking the performance of a full-scale building envelope assembly with its scaled-down prototype, it would not be feasible to evaluate the dynamic thermal performance of building envelopes using small-scale hot box apparatus. In this light, in order to circumvent limitations of large-scale hot box tests, this research aims to develop the scaling relationships between full-size and scaled-down hot box tests to enable the evaluation of both steady-state and dynamic thermal properties of building envelop components through affordable small-scale hot box apparatus. First, the theoretical relationship between the dynamic thermal properties of scaled-down specimen and their corresponding full-size specimen were established based on Laplace transformation. The equivalence conditions for dynamic thermal properties between the EN ISO 13768 method (ISO method) and the finite difference method were established. Meanwhile, a low-cost, small-scale calibrated hot box apparatus was developed, which comprises an insulated five-sided box (hot-side), a programmable environmental chamber (cold-side), and a hot-side box equipped with a programmable heater and a varying-speed crossflow fan. Experimental tests conducted on three scaled-down insulated concrete sandwich panels, together with the simulated thermal response of their full-scale counterparts, indicate that the proposed method provides a convenient and low-cost experimental evaluation method for promoting the development and innovation of new building envelope materials and design concepts using scaled-down prototypes.

2. Evaluating thermal performance of building envelope using scaled-down tests

2.1. Formulations

For a multi-layer wall assembly (Fig. 1), its indoor and outdoor surfaces are exposed to a combination of convection and radiation, represented by h_{si} and h_{so}. T_{ai} and T_{ao}, respectively, represent the indoor and outdoor air temperatures (see Fig. 1). Assuming there is no heat generation in the wall and the thermophysical properties of the material are constant, the governing Equation for 1-D heat transfer within the k-th layer of an N-layer wall assembly is:

$$-\chi_k \frac{\partial T(x,t)}{\partial x} = q \tag{1}$$

$$\alpha_k \frac{\partial^2 T(x,t)}{\partial x^2} = \frac{\partial T(x,t)}{\partial t} \tag{2}$$

where $\alpha_k = \frac{\chi_k}{\rho_k c_{p,k}}$ is the thermal diffusivity of the k-th layer; $\chi$is the thermal conductivity, T is the temperature which is a function of time, t, and space, x; ρ and c_p are the density and specific heat of the material, respectively.

The Laplace transformation of Equations (1) and (2) yields:

$$-\chi \frac{\partial \bar{T}(x,s)}{\partial x} = \bar{q}(x,s) \tag{3}$$

$$\chi \frac{\partial^2 \bar{T}(x,s)}{\partial x^2} = \rho c_p \left[s\bar{T}(x,s) - T(x,0) \right] \tag{4}$$

where s is a complex variable, $s = \tau + j\omega$; $\bar{T}(x,s) = Laplace(T(x,t)) = \int_0^\infty e^{-st} T(x,t)dt$ and $\bar{q}(x,s) = Laplace(q(x,t)) = \int_0^\infty e^{-st} q(x,t)dt$. Supposing initial condition $T(x,0) = 0$ and solving Equation (4) yields:

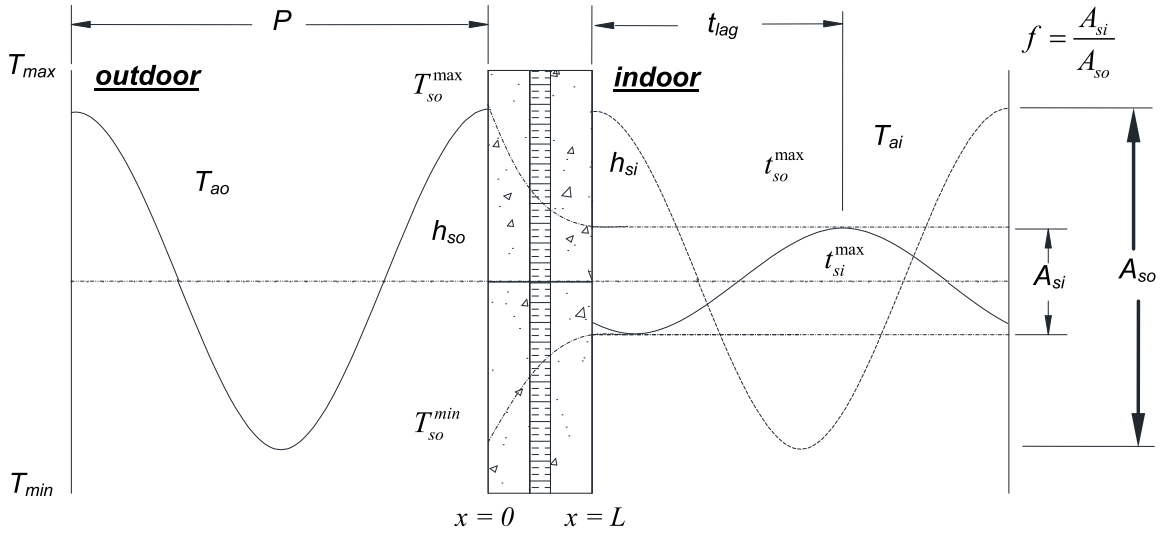

Fig. 1. Transient temperatures and heat flux going through a multi-layer wall panel.

$$\bar{T}(x,s) = C_1 e^{\sqrt{\frac{s\rho c_p}{\chi}}x} + C_2 e^{-\sqrt{\frac{s\rho c_p}{\chi}}x} \tag{5}$$

where C_1 and C_2 are constants to be determined by boundary conditions.

Substituting Equation (5) into Equation (3) leads to:

$$\bar{q}(x,s) = -C_1\sqrt{s\chi\rho c_p}e^{\sqrt{\frac{s\rho c_p}{\chi}}x} + C_2\sqrt{s\chi\rho c_p}e^{-\sqrt{\frac{s\rho c_p}{\chi}}x} \tag{6}$$

Applying the boundary conditions at outdoor surface 1: $\bar{T}_1(s) = \bar{T}(0,s)$, $\bar{q}_1(s) = \bar{q}(0,s)$, and at indoor surface 2: $\bar{T}_2(s) = \bar{T}(L,s)$, $\bar{q}_2(s) = \bar{q}(L,s)$ to Equations (5) and (6) we have [32,33]:

$$\begin{Bmatrix} \bar{T}_2(s) \\ \bar{q}_2(s) \end{Bmatrix} = \begin{bmatrix} Z_{11} & Z_{12} \\ Z_{21} & Z_{22} \end{bmatrix}_k \begin{Bmatrix} \bar{T}_1(s) \\ \bar{q}_1(s) \end{Bmatrix} = \begin{bmatrix} \cosh\psi & -\frac{\sinh\psi}{Z_0} \\ -Z_0\sinh\psi & \cosh\psi \end{bmatrix}_k \begin{Bmatrix} \bar{T}_1(s) \\ \bar{q}_1(s) \end{Bmatrix} \tag{7}$$

where $\psi = \sqrt{\frac{\rho c_p s}{\chi}}L$, and $Z_0 = \sqrt{\rho c_p \chi s}$. Note that for a sinusoidal excitation ($s = j\omega$), equation (7) takes the same form as in [8], where:

$$\psi = (1+j)\xi = (1+j)\sqrt{\frac{\omega\rho c_p}{2\chi}}L \tag{8}$$

and

$$Z_0 = \sqrt{\frac{\omega\chi\rho c_p}{2}}(1+j) \tag{9}$$

For a scaled-down (SD) specimen having a dimension ratio of $n = L^{SD}/L$ with respect to the full-size specimen, ξ in Equation (8) is written as:

$$\xi_{SD} = nL\sqrt{\frac{\omega^{SD}\rho c_p}{2\chi}} \tag{10}$$

If the scaled-down specimen is made from the same materials as the full-size prototype, for $\xi^{SD} = \xi$, the temperature frequency at which the scaled-down specimens are exposed to on the exterior surface should satisfy the relationship:

$$\omega^{SD} = \frac{1}{n^2}\omega \tag{11}$$

2.1.1. Single-layer wall panels

For wall (roof) panel specimens having only one layer of material, the periodic thermal transmittance, Y_{12}, can be obtained by assuming sinusoidal excitation on the exterior surface and isothermal condition (T_2 = 0) on the interior surface:

$$Y_{12} = \left(\frac{\hat{q}_2}{\hat{T}_1}\right)_{\hat{T}_2=const} = -\frac{1}{Z_{12}} = \frac{Z_0}{\sinh(\xi+j\xi)} = \frac{\sqrt{\frac{\omega\chi\rho c_p}{2}}(1+j)}{\sinh(\xi+j\xi)} \tag{12}$$

When the frequency of excitation temperature ω^{SD} satisfies the relationship of Equation (11), the thermal transmittance, Y_{12}^{SD}, evaluated using a scaled-down specimen is:

$$Y_{12}^{SD} = \frac{\sqrt{\frac{\omega^{SD}\chi\rho c_p}{2}}(1+j)}{\sinh(\xi+j\xi)} = \frac{1}{n}\frac{\sqrt{\frac{\omega\chi\rho c_p}{2}}(1+j)}{\sinh(\xi+j\xi)} = \frac{1}{n}Y_{12} \tag{13}$$

Therefore, the time lag, t_{lag}, evaluated using a scaled-down specimen is related to the full-size prototype by the relationship of:

$$t_{lag}^{SD} = \frac{1}{\omega^{SD}}\arg\left(-\frac{1}{Y_{12}^{SD}}\right) = \frac{n^2}{\omega}\arg\left(-\frac{n}{Y_{12}}\right) = n^2 t_{lag} \tag{14}$$

Note that the thermal transmittance (U-value) across the specimen is:

$$U_0 = \frac{1}{R_{si}+R_{so}+R} \tag{15}$$

where $R = L/\chi$ is the thermal resistance of the specimen; R_{si} and R_{so} are surface resistances on the indoor and outdoor sides, respectively. If the surface resistances (R_{si} and R_{so}) are small in comparison with R ($R_{si}+R_{so} \ll R$), we will have:

$$U_0^{SD} = \frac{1}{R_{si}^{SD}+R_{so}^{SD}+nR} \approx \frac{1}{n}U_0 \tag{16}$$

Otherwise, the surface resistances of the scaled specimen need to be tuned so that $\left(R_{si}^{SD}+R_{so}^{SD}\right) \approx n(R_{si}+R_{so})$ for the relationship in Equation (16) to hold. Under such conditions, the decrement factor, f, (Fig. 1) evaluated using a scaled-down specimen is correlated to those of the full-size prototype by:

$$f^{SD} = \frac{\left|Y_{12}^{SD}\right|}{U_0^{SD}} \approx \frac{\left|n\left(-\frac{1}{Z_{12}}\right)\right|}{nU_0} = f \tag{17}$$

2.1.2. Multi-layer building envelope assembly

For a multi-layer wall assembly having N layers, the heat flux and temperature on the indoor surface is related to those on the outdoor surface by:

$$\begin{pmatrix} \bar{T}_2 \\ \bar{q}_2 \end{pmatrix} = \boldsymbol{Z}^N \boldsymbol{Z}^{N-1} \cdots \boldsymbol{Z}^2 \boldsymbol{Z}^1 \begin{pmatrix} \bar{T}_1 \\ \bar{q}_1 \end{pmatrix} = \begin{bmatrix} Z_{11} & Z_{12} \\ Z_{21} & Z_{22} \end{bmatrix}_{overall} \begin{pmatrix} \bar{T}_1 \\ \bar{q}_1 \end{pmatrix} \tag{18}$$

The heat transfer matrix of a scaled-down N-layer wall assembly is correlated to that of the full-size prototype by:

$$\boldsymbol{Z}_{overall}^{SD} = \boldsymbol{Z}_1^{SD} \boldsymbol{Z}_2^{SD} \cdots \boldsymbol{Z}_N^{SD} = \begin{bmatrix} Z_{11}^{SD} & Z_{12}^{SD} \\ Z_{21}^{SD} & Z_{22}^{SD} \end{bmatrix}_{overall} = \begin{bmatrix} Z_{11} & \frac{1}{n} Z_{12} \\ nZ_{21} & Z_{22} \end{bmatrix}_{overall} \tag{19}$$

Thus, the time lag of a scaled-down multi-layer wall assembly is related to its full-scale counterpart by:

$$\begin{aligned} t_{lag,overall}^{SD} &= \frac{1}{\omega^{SD}} \arg\left(Z_{12,overall}^{SD}\right) = \frac{n^2}{\omega} \arg\left(nZ_{12,overall}\right) \\ &= n^2 t_{lag,overall} \end{aligned} \tag{20}$$

The U-value of a scaled N-layer assembly is:

$$U_{overall}^{SD} = \frac{1}{R_{si}^{SD} + R_{so}^{SD} + \sum_{i=1}^{N} R_i^{SD}} \tag{21}$$

Similarly, if $R_{si} + R_{so} \ll \sum R_i$ or $\left(R_{si}^{SD} + R_{so}^{SD}\right) \approx n(R_{si} + R_{so})$, we have $U_{overall}^{SD} \approx \frac{1}{n} U_{overall}$. In such a case, the decrement factor of a scaled-down specimen is the same as that of a full-size prototype:

$$f_{overall}^{SD} = \frac{\left|\frac{1}{n}\left(-\frac{1}{Z_{12,overall}}\right)\right|}{\frac{1}{n} U_{overall}} = f_{overall} \tag{22}$$

It is noted that the deduction above adopted a similar method that was used in EN ISO 13,768 method (ISO method), while the ISO method was extended to account for the scaling relationships between full-size and scaled-down specimens.

2.2. Finite difference simulation

In this research, the finite difference (finite volume) method is also used to simulate the 1-D heat transfer through the concrete sandwich wall panels. The finite difference (FD) simulation will be experimentally validated at reduced scale and used to simulate the dynamic thermal behavior of full-scale building envelopment components. Fig. 2 shows the finite volume discretization of three-layer concrete sandwich wall panels. Considering an arbitrary internal node i located at the location x_i and its two contiguous nodes to the left and right of node i are i-1 and i + 1, and their locations are x_{i-1} and x_{i+1}. The finite volume solution takes the form of [34]:

$$a_i T_i = b_i T_{i+1} + c_i T_{i-1} + d_i \tag{23}$$

where coefficients a_i, b_i, c_i, and d_i are listed in Table 1 for different types of nodes.

The time lag, t_{lag}^{FD}, refers to the time required for the heat wave to propagate from the outdoor surface to the indoor surface and is determined as the phase lag between the outdoor surface temperature, $t_{so}^{\max}$, and the temperature response measured from the indoor panel surface, $t_{si}^{\max}$ (see Fig. 1):

$$t_{lag}^{FD} = t_{si}^{\max} - t_{so}^{\max} \tag{24}$$

where $t_{si}^{\max}$ and $t_{so}^{\max}$ are the times at which the indoor surface (si) and the outdoor surface (so) reaches their peak temperatures, respectively. The decrement factor, f^{FD}, is determined as the decreasing ratio of their amplitude during this process, see Fig. 1:

$$f^{FD} = \frac{Amp_{si}}{Amp_{so}} = \frac{T_{si}^{\max} - T_{si}^{\min}}{T_{so}^{\max} - T_{so}^{\min}} \tag{25}$$

where Amp_{si} and Amp_{so} represent the amplitude of the indoor and outdoor surface temperature fluctuations, respectively. It is worth noting that superscripts, i.e., *EXP*, *FD*, and *ISO*, represent the dynamic thermal properties obtained by experiment, finite difference method, and the ISO method, respectively.

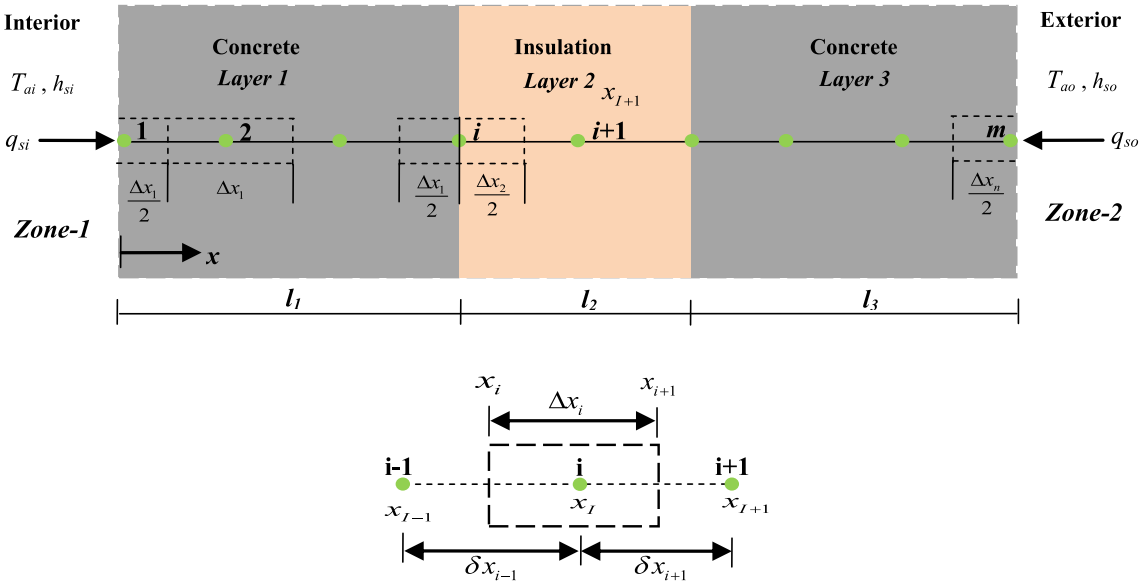

Fig. 2. Finite volume discretize of a three-layer concrete sandwich wall panel.

Table 1
Coefficients used in the finite difference method for 1D heat transfer simulation.

Type of node	a_i	b_i	c_i	d_i
Node 1	$1+2\frac{\alpha_k\Delta t}{(\delta x_{i+1})^2}+2\frac{\alpha_k\Delta t}{(\delta x_{i+1})^2}\frac{h_{si}(\delta x_{i+1})}{\gamma_k}$	$2\frac{\alpha_k\Delta t}{(\delta x_{i+1})^2}$	0	$T_i^{old}+2\frac{\alpha_k\Delta t}{(\delta x_{i+1})^2}\frac{h_{si}(\delta x_{i+1})}{\gamma_k}T_{ai}$
Interior Node	$1+2\frac{\alpha_k\Delta t}{(\Delta x_i)^2}$	$\frac{\alpha_k\Delta t}{(\Delta x_i)^2}$	$\frac{\alpha_k\Delta t}{(\Delta x_i)^2}$	T_i^{old}
Interface Node	$\frac{\rho_k c_k\delta x_{i-1}+\rho_{k+1}c_{k+1}\delta x_{i+1}}{2\Delta t}+\frac{\gamma_k}{\delta x_{i-1}}+\frac{\gamma_{k+1}}{\delta x_{i+1}}$	$\frac{\gamma_{k+1}}{\delta x_{i+1}}$	$\frac{\gamma_k}{\delta x_{i-1}}$	$\left(\frac{\rho_k c_k\delta x_{i-1}+\rho_{k+1}c_{k+1}\delta x_{i+1}}{2\Delta t}\right)T_i^{old}$
Node m	$1+2\frac{\alpha_k\Delta t}{(\delta x_{i-1})^2}+2\frac{\alpha_k\Delta t}{(\delta x_{i-1})^2}\frac{h_{so}(\delta x_{i-1})}{\gamma_k}$	0	$2\frac{\alpha_k\Delta t}{(\delta x_{i-1})^2}$	$T_i^{old}+2\frac{\alpha_k\Delta t}{(\delta x_{i-1})^2}\frac{h_{so}(\delta x_{i-1})}{\gamma_k}T_{ao}$

2.3. Equivalence between ISO method and finite difference method

2.3.1. Time lag

For the scaled-down (SD) specimen to represent a similar cyclic thermal response of the full-size component, the period for the harmonic forcing temperature should satisfy the relationship of Equation (11). For example, for a ½ scale model specimen to represent the behavior of a full-scale wall exposed to a 24-hour temperature cycle, the period for the forcing temperature cycling imposed on the scaled-down specimen should be at 6 h (¼th of 24 h). As discussed in prior sections, when the period of forcing temperature satisfies the condition described in Equation (11), the time lag tested by the scaled-down specimen should be correlated to its full-size counterpart by Equation (14). However, the time lag obtained from finite difference simulation, as calculated by Equation (24), implicitly depends on the indoor boundary conditions, i.e., the effect of the indoor surface convection coefficient, h_{in}. For Equation (14) to match the finite different simulation results, the indoor surface convection should be modeled as a boundary surface layer [8]. In the case of a single layer wall panel, Equation (7) can be expressed as:

$$\begin{Bmatrix}\bar{T}_2(s)\\ \bar{q}_2(s)\end{Bmatrix}=\begin{bmatrix}1 & -R_{si}\\ 0 & 1\end{bmatrix}\begin{bmatrix}Z_{11} & Z_{12}\\ Z_{21} & Z_{22}\end{bmatrix}\begin{Bmatrix}\bar{T}_1(s)\\ \bar{q}_1(s)\end{Bmatrix} \tag{26}$$

where R_{si} is the surface resistance of the boundary layer with $R_{si}=1/h_{si}$. Then, Equation (12) can be rewritten as:

$$Y_{12}=\left(\frac{1}{1+\frac{\sqrt{\frac{\omega\gamma\rho c}{2}}(1+j)}{h_{si}^{FS}}\coth(\xi+j\xi)}\right)\frac{\sqrt{\frac{\omega\gamma\rho c}{2}}(1+j)}{\sinh(\xi+j\xi)} \tag{27}$$

For a scaled-down specimen, Equation (13) can be rewritten as:

$$Y_{12}^{SD}=\left(\frac{1}{1+\frac{\sqrt{\frac{\omega^{SD}\gamma\rho c}{2}}(1+j)}{h_{si}^{SD}}\coth(\xi+j\xi)}\right)\frac{1}{n}\frac{\sqrt{\frac{\omega\gamma\rho c}{2}}(1+j)}{\sinh(\xi+j\xi)} \tag{28}$$

Comparing Equations (27) and (28), we have $Y_{12}^{SD}=\frac{1}{n}Y_{12}$ when:

$$\frac{\sqrt{\omega^{SD}}}{h_{si}^{SD}}=\frac{\sqrt{\omega}}{h_{si}^{FS}} \tag{29}$$

Therefore, in order for the time-lag obtained by Equation (14) and Equation (24) to be equal, one should have:

$$(h_{si}/U_0)^{SD}=(h_{si}/U_0)^{FS} \tag{30}$$

2.3.2. Decrement factor

On the other hand, the ISO equations calculate the decrement factor through the relationship [8]:

$$f^{ISO}=\frac{|\hat{q}_{si}|}{\left|\hat{T}_{so}\right|\times U_0} \tag{31}$$

where $\hat{q}_{si}$ is the magnitude of indoor surface heat flow and $\hat{T}_{so}$ is its corresponding outdoor surface temperature.

Considering the convective heat transfer at the indoor surface, Equation (31) may be rewritten as:

$$f^{ISO}=\frac{q_{si}^{\max}-q_{si}^{\min}}{(T_{so}^{\max}-T_{so}^{\max})\times U_0}=\frac{h_{si}(T_{si}^{\max}-T_{ai})-h_{si}\left(T_{si}^{\min}-T_{ai}\right)}{\left(T_{so}^{\max}-T_{so}^{\min}\right)\times U_0} \tag{32}$$

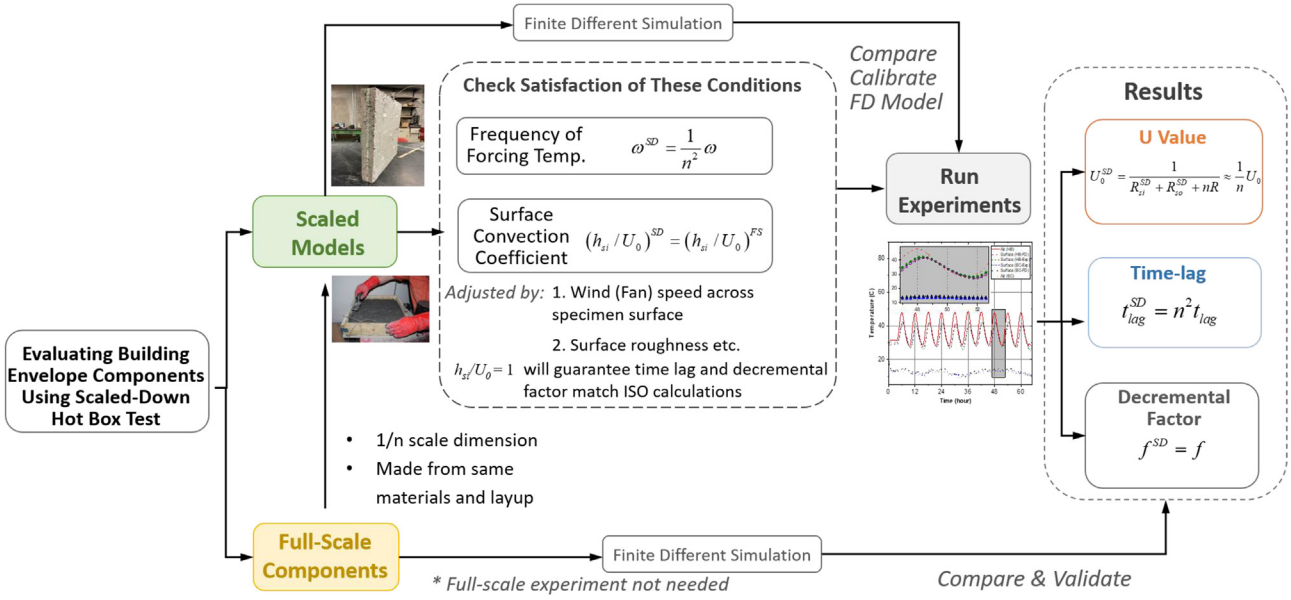

Fig. 3. Flow chat summarizing the evaluation procedure using scaled hot box test.

where q_{si}^{max} and q_{si}^{min} are the maximum and minimum of indoor heat flow, respectively.

Assuming indoor surface convection coefficient h_{si} remains a constant during the experiment/ simulation, Equation (32) can be simplified as:

$$f^{ISO} = \frac{h_{si}}{U_0}\frac{\left(T_{si}^{max} - T_{si}^{min}\right)}{\left(T_{so}^{max} - T_{so}^{max}\right)} \tag{33}$$

Comparing Equation (33) with Equation (25), it is evident that a factor of h_{si}/U_0 relates to the decrement factor obtained by the ISO method and FD method. For Equation (33) and Equation (25) to be equivalent, one should have $h_{si}/U_0 = 1$; otherwise, the decrement factor obtained by the experiment or finite difference simulation is scaled by a factor of h_{in}/U_0 as compared to that calculated by the ISO method [8]. For a scaled-down experiment, for the decrement factor to satisfy the correlation described by Equation (17), we also should have the condition $(h_{si}/U_0)^{SD} = (h_{si}/U_0)^{FS}$ (Equation (30)).

Fig. 3 presents a flow chart summarizing the procedure to test the dynamic thermal performance of building envelope components using scaled-down hot box tests, where the test conditions and scaling relationships between responses obtained from the scaled-down models and their corresponding full-scale prototype are outlined.

3. Small-scale calibrated hot box apparatus setup and calibration

3.1. Instrumentation and setup

In this section, a small-scale hot box apparatus with a 355 mm by 355 mm (14 in by 14 in) open test area was developed and calibrated. The overall dimensions of the designed hot-side are 445 mm × 445 mm × 380 mm (17.5 in × 17.5 in × 15 in) in *x*-*y*-*z* directions (see Fig. 4 (b)). The hot-side box consists of a five-sided insulated box with a programmable DC power supply (Rigol DP832), a fin-heater, and a variable-speed crossflow fan. The programmable DC power source has built-in sine, pulse, and ramp control functions. The cold-side environmental chamber is equipped with temperature and relative humidity conditioning and programmable control, which can simulate a range of temperature and humidity profiles. An insulated specimen frame is clamped between the chambers, see Fig. 4. The hot-side box is also instrumented and calibrated as a metering chamber to measure the thermal flow through the test specimens. The box is constructed using 25.4 mm (1 in)-thick rigid closed-cell foam board, finished with 19.1 mm (¾ in) thick plywood backings and a layer of an insulation blanket. The insulation blanket reduces the influence of temperature fluctuation in the laboratory. An aluminum baffle, 3 mm thick by 305 mm wide by 305 mm high, is vertically placed in the center of the hot-side box to direct the airflow to the surface of the test specimen, see Fig. 4 (b). The baffle is located at 121 mm (4.75 in) from the test specimen surface and about 230 mm (9 in) from the crossflow fan. The fin-heater is raised above the bottom of the baffle, which shields the test specimen from direct radiation of the heater. As a result, heated air flows up between the sample surface and the baffle through the gap at the bottom and then returns through the opening at the top. In this way, an air loop is formed in the metering chamber, reducing the potential non-uniform heating on the test specimen [35]. Type K thermocouples (Omega SA1XL-K, with accuracy ± 0.2 °C or 0.75%) were used to measure the temperatures. Five type K thermocouples and one type K thermocouple were attached on the backside and the remaining four sides of the metering walls (total of 18

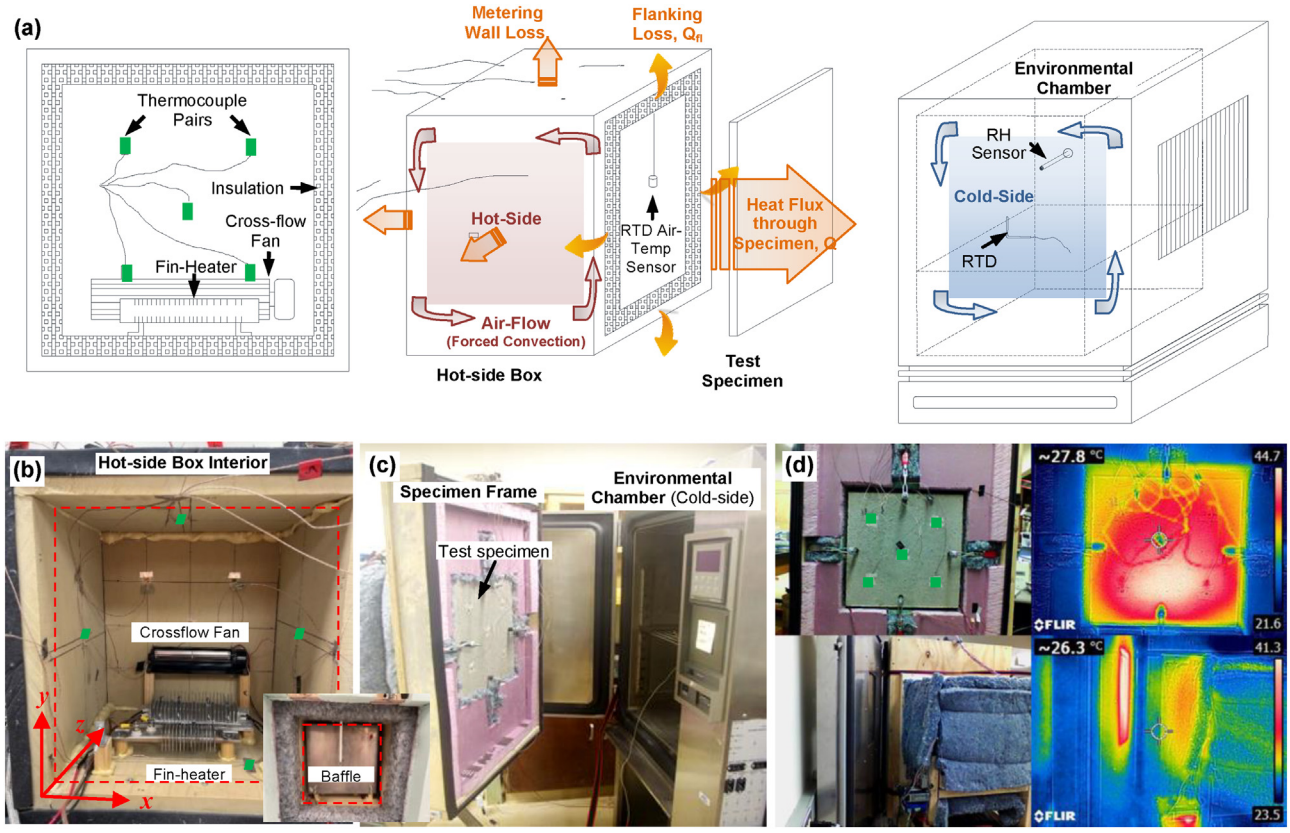

Fig. 4. Hot box setup and instrumentation: (a) schematic figures showing the setup of hot box (hot-side), heat losses, and the environment chamber (cold-side); (b) pictures showing the instrumentation of the hot-side box (metering chamber); (c) picture showing the specimen frame and its interface with the environment chamber (cold-side); and (d) infrared thermal images showing the heat flow through the specimen and heat loss (flanking loss and frame loss).

locations inside and 18 locations outside the box, see Fig. 4 (b)), respectively. Thus, heat flux going through the metering walls can be calculated from the measured temperature differential. Instrumentation is also provided to measure the total energy input into the hot box (i.e., heating and fan). The heat losses are determined by calibrating the box with panel specimens of known thermal properties (R-value), detailed in the following section.

The hot- and cold-side air temperature was measured with a set of RTD sensors (Omega RTD-805). A fan circulated air in the cold-side chamber, and the air temperature was controlled by the built-in controller of the environmental chamber. At the same time, an additional RTD sensor and a relative humidity (RH) sensor (Omega HX92B) were mounted near the specimen surface to directly measure the air temperature and RH level near the specimen panel. All data collection sensors were conditioned using a *National Instrument* PXI-express DAQ system with adjustable data sampling frequency up to 100 samples/sec. During steady-state tests, a constant power input was supplied to the DC heater in the hot-side box. The air temperature in the environmental chamber (cold-side) was maintained constant as well. The temperature profile of each side could be individually controlled if the dynamic thermal performance of the building envelope element specimens were to be tested. In addition, a FLIR E5XT thermal imaging inspection camera was used to collect thermal images during experimental tests.

3.2. Calibration

A homogenous rigid foam panel specimen with known thermophysical properties was tested under steady-state conditions to calibrate the hot box apparatus. The thermophysical properties (i.e., thermal conductivity and specific heat) of the rigid foam panel and materials used for constructing the small-scale hot box apparatus were measured by the Transient Plane Source (TPS) method using a *Hotdisk TPS 1500* thermal constant analyzer [36]. The calibration of the small-scale hot box apparatus was carried out by balancing the energy components following the procedure outlined in ASTM C1363 [37], where the fin-heater and the crossflow fan were considered as the energy input into the hot-side box. The total energy input is the summation of the programmed electricity energy supplied to the heaters recorded by the NI PXI DAQ system and the energy consumed by the fan measured by an inline power meter. The system energy losses are subtracted from the total energy input to calculate thermal energy passing through the tested specimen (i.e., rigid foam panel).

A total of three energy loss components were considered based on the geometries of the hot box, sample holder, and surrounding frame, including the metering wall heat loss (Q_{mw}), flanking heat loss (Q_{fl}), and the heat loss from frame/foam (Q_{ff}). The frame/foam loss was added to account for heat losses due to the geometry of the hot box developed herein, which is different from the ASTM standard configuration. Foam loss refers to the heat loss due to the contact of the insulated specimen frame to the cold-side chamber. The frame loss refers to the heat loss due to the sample supports and clamp mounts. Fig. 4 (d) shows the thermal loss associated with the specimen frame.

Since the thermal properties of the metering wall materials are known (experimentally measured by the TPS method), the metering wall loss, Q_{mw}, is calculated based on the readings of thermocouple pairs and can be calculated as [37]:

$$Q_{mw} = \frac{\chi_{eff-mw} A_{eff-mw} (T_{si-mw} - T_{so-mw})}{L_{mw}} \tag{34}$$

where $\chi_{eff\text{-}mw}$ is the effective thermal conductivity of the metering wall, $T_{si\text{-}mw}$ and $T_{so\text{-}mw}$ are the inside, and outside wall surface temperatures respectively, L_{mw} is the wall thickness, and $A_{eff\text{-}mw}$ is the effective area normal to heat flow which can be calculated by:

$$A_{eff-mw} = A_{si-mw} + 0.54 L_{mw} \left(\sum el_p \right) + 0.60 L_{mw}^2 \tag{35}$$

with $A_{si\text{-}mw}$ is the inside surface area of the metering chamber, Σel_p is interior edge lengths of the metering chamber where walls meet, and the coefficients 0.54 and 0.15 (0.60 = 0.15 × 4) are the conduction shape factors for metering wall interior edges and the thickness of the metering wall respectively [38].

The flanking wall loss is estimated where a FLIR infrared thermal camera is used to measure the external temperature, (see Fig. 4 (d)). The flanking loss (Q_{fl}) can be calculated as:

$$Q_{fl} = \chi_{eff-fl} \left(A_{eff-fl} / L_{eff-fl} \right) \Delta T_{ai-ao} \tag{36}$$

where $\chi_{eff\text{-}fl}$ is the effective thermal conductivity of base insulation and the skin material, $A_{eff\text{-}fl}/L_{eff\text{-}fl}$ is the effective area/path length of the entire frame around its perimeter, and $\triangle T_{ai\text{-}ao}$ is the air-to-air temperature difference between inside and outside.

The frame and foam heat loss (Q_{ff}) can be calculated as:

$$Q_{ff} = \frac{A_{frame}}{R_{frame}} \left(T_{si-frame} - T_{so-frame} \right) + \frac{A_{foam}}{R_{foam}} \left(T_{si-foam} - T_{so-foam} \right) \tag{37}$$

where A_{frame}, A_{foam}, R_{frame}, R_{foam}, $T_{si\text{-}frame}$, $T_{si\text{-}foam}$, and $T_{so\text{-}frame}$, $T_{so\text{-}foam}$, are the surface area, thermal resistance, and inside and outside surface temperatures of the frame and foam, respectively.

By subtracting all losses from the total input energy into the system, the total heat flowing through the specimen can be determined. The R-value of the test specimen (R_{sp}) can then be calculated by:

$$R_{sp} = \frac{A_{sp}}{Q_{input} - Q_{loss}} \left(T_{sp-hot} - T_{sp-cold} \right) \tag{38}$$

Table 2
Energy input, loss, and test panel R-value.

$A_{eff\text{-}mw}$	L_{mw}	$\sum el_p$	$T_{so\text{-}mw}$	30.3 °C	Q_{mw}
0.201 m^2	0.045 m	3.048	$T_{si\text{-}mw}$	37.6 °C	6.785 W
A_{eff}	0.201 m^2		λ_{eff}	0.205 W/mK	
$L_{eff\text{-}fl}$	1.78m		$T_{so\text{-}fl}$	17.0 °C	Q_{fl}
					0.595 W
A_{frame}	R_{frame}		$T_{si\text{-}frame}$	37.1 °C	Q_{ff}
0.062 m^2	0.214 m^2K/W		$T_{so\text{-}frame}$	26.0 °C	3.741 W
A_{foam}	R_{foam}		$T_{si\text{-}foam}$	37.6 °C	
0.011 m^2	0.258 m^2K/W		$T_{so\text{-}foam}$	28.8 °C	
Q_{input}		16.654 W		Q_{loss}	11.121 W
A_{sp}	$T_{sp\text{-}hot}$	$T_{sp\text{-}cold}$		Q_{input}-Q_{loss}	R_{sp}
0.126 m^2	36.4 °C	13.1 °C		5.533 W	0.5582

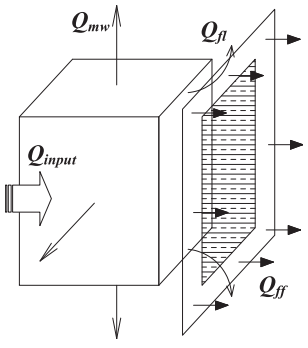

Table 3
Thermal properties of concrete materials [39]

Concrete ID	Density	Thermal Conductivity	Thermal Diffusivity	Volumetric Heat Capacity
	Kg/m^3	W/mK	mm2/s	kJ/m^3
C1 (NS-FAC/RLF-RLC*)	1224	0.423	0.334	1267
C2 (NS-SS-RLC*)	1614	1.050	0.717	1464
C3 (NS-SS-G*)	2185	1.817	0.954	1904

* represents the Mix ID in reference [39].

Table 2 summarizes the calibration result by using a rigid foam panel with known thermal properties. It includes the hot box's geometry and thermophysical properties, the specimen, the measured temperature readings, energy losses, and the R-value of the specimen calculated by using Equations (34) – (38). As can be seen, the R-value obtained by the hot box test matches well with the R-value calculated based on the thermal conductivity value tested by TPS with 0.5329 m^{2}K/W.

4. Thermal performance characterization of wall panels

4.1. Specimen design

Following the calibration process, three scaled-down concrete sandwich wall panels were prepared and tested under periodically transient conditions (i.e., sinusoidal temperature wave) using the small-scale calibrated hot box. Data obtained by the transient tests were used to calculate the dynamic thermal response of the wall assemblies based on the equations derived in Section 2.

In this study, three concrete sandwich wall panels made from normal-weight concrete, structural lightweight concrete, and low-density cementitious composites [39] were prepared and tested. The physical and thermal properties of concretes used to construct the sandwich wall panels are summarized in Table 3. The concrete mixture design was presented in a previous paper by the authors [39]. Three different concrete types were selected in this study, i.e., C1 and C2 represent lightweight concrete while C3 represents normal weight concrete. The difference between C1 and C2 is that the mixture of C1 also added fly-ash cenospheres (FAC) to further reduce the concrete's density and thermal conductivity. The densities of C1 to C3 ranged from 1224 to 2387 kg/m^3 (oven-dry condition), with thermal conductivity measured by the transient plane source (TPS) method [40] ranged from 0.423 to 1.817 W/m-K. Fig. 5 presents the preparation process, configuration, and instrumentation of the scaled-down insulation concrete sandwich panels. The test panels consist of one layer of 15.9 mm thick rigid expanded polystyrene (EPS) foam board sandwiched between two layers of concrete wythes (25.4 mm thick for each layer). A layer of wire mesh (50 mm by 50 mm spacing) (2 in × 2 in) was used as reinforcements for the concrete layers, and U-type steel connectors were used to connect the two concrete wythes and provide sheer resistance. The prepared insulated concrete sandwich panels present one half (1/2) scale of a typical concrete sandwich wall panel with an overall thickness of 127 mm (5

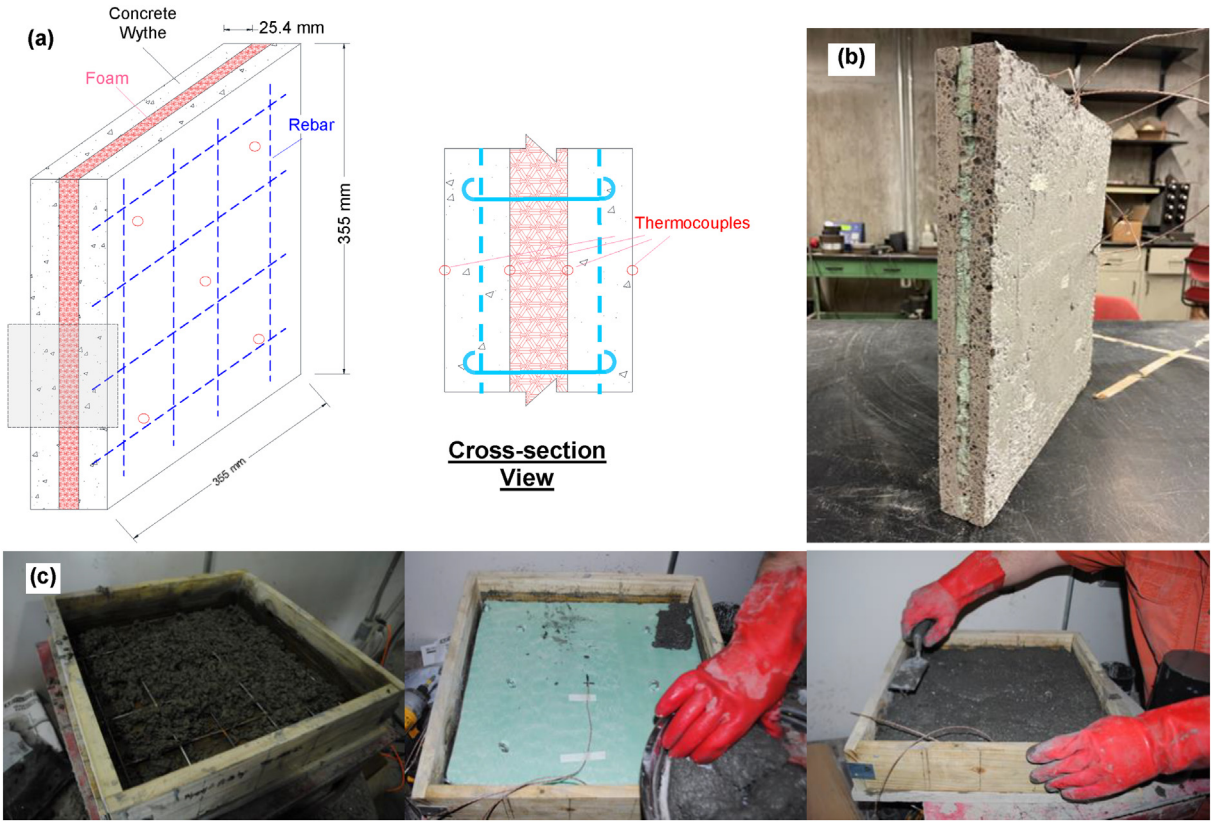

Fig. 5. The scaled-down concrete sandwich wall panel specimen: (a) Illustrative figure showing the configuration and instrumentation; (b) picture showing the cross-section of the specimen panel; and (c) pictures showing the specimen preparation process.

in). Five thermocouples were attached on the front and back surfaces of the tested specimens, respectively (see Fig. 5 (a)). Moreover, thermocouples were also attached to the surfaces of the insulation panel to monitor the temperature development history during the experimental test and validate the finite difference method presented in *Section 2.2*, see Fig. 5 (b) and (c). Table 4 summarizes the design and dimensions of each panel.

4.2. Transient thermal behavior of scaled-down concrete sandwich wall panels

Fig. 6 presents the experimental data obtained by the small-scale hot box apparatus. According to Equation (14), the temperature of the hot-side box follows a sinusoidal temperature profile with the period, *P*, equals to 6 h to account for the ½ scale factor (to represent a 24-hour test cycle for a full-scale specimen). On the cold side, the environmental chamber air temperature was kept at a constant temperature at around 15 °C. During the experiment, both the hot- and cold-side were pre-heated or cooled to a pre-designated temperature (close to steady-state), followed by the sinusoidal forcing temperature solicitation. As can be seen from the experimental data, the hot-side air temperature history follows the sinusoidal input temperature closely. In contrast, the cold-side air temperature experienced some disturbances due to the limitation of the environmental chamber's control program. Therefore, data segments with environmental chamber temperature close to a constant were used to calculate the dynamic properties, i.e., time lag (t_{lag}^{EXP}) and decremental factor (f^{EXP}).

Fig. 6 presents the hot box test data obtained by the experiment compared to the simulated results obtained using the finite difference (FD) method. It can be seen that once the stabilized periodic regime is reached, the simulated data matches closely with the experimental data. The thermal properties of the tested panels are presented in Fig. 7, where the LLL panel has the lowest U-value. The NNL panel has a smaller time lag, but a larger decrement factor than the NNN panel indicates the influence of thermal mass on dynamic thermal properties (see Fig. 7 (b) and (c)). Table 5 compares the time lag and decrement factor obtained from the experimental data, the finite difference simulations, and those calculated from the ISO method. The time lag and decrement factor obtained from the FD method and experimental tests were deducted from the same equations – i.e., Equations (24) and (25). The measured

Table 4
Concrete sandwich wall panel composition and thermal transmittance.

Sandwich panel	Component composition (hot to cold side)	Calculated thermal transmittance (W/m^{2}K)
LLL	2.54 cm C1; 1.59 cm EPS; 2.54 cm C1	1.934
NNL	2.54 cm C2; 1.59 cm EPS; 2.54 cm C2	2.246
NNN	2.54 cm C3; 1.59 cm EPS; 2.54 cm C3	2.354

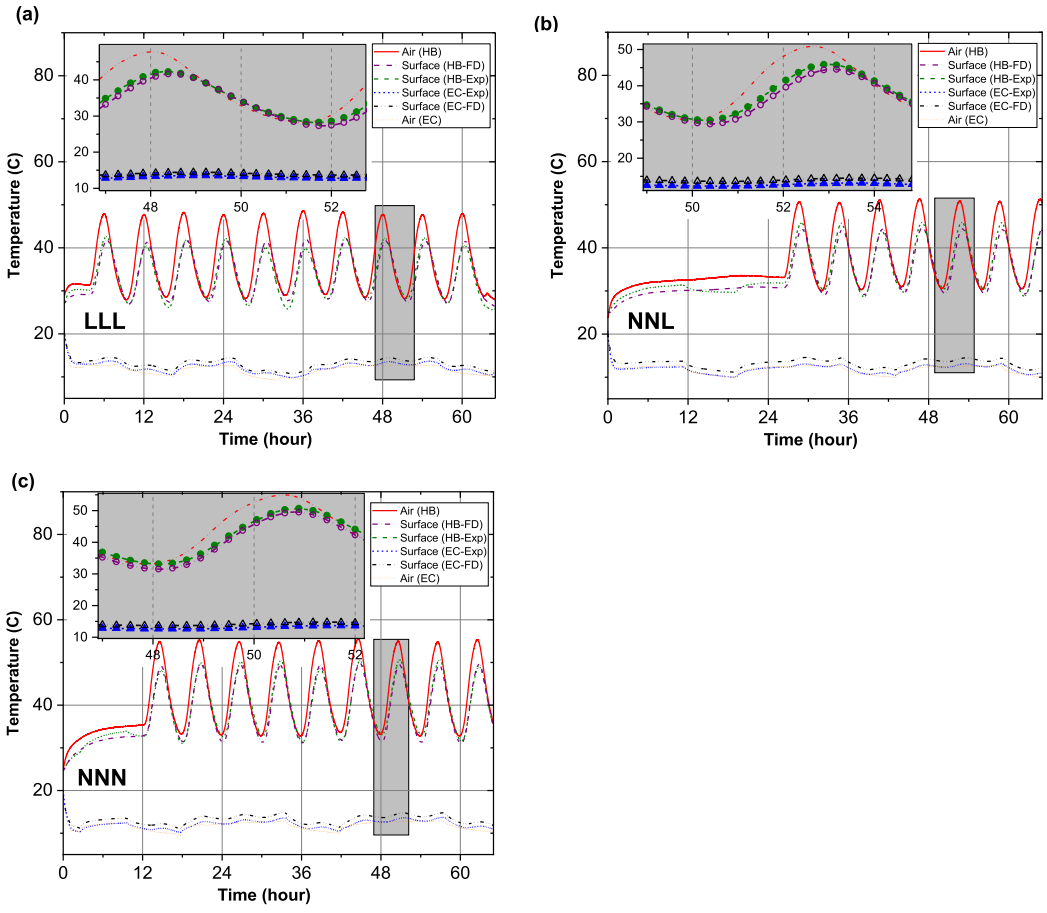

Fig. 6. Hot box testing results versus finite different method simulated results and thermal properties of tested panels: (a) LLL; (b) NNL; and (c) NNN.

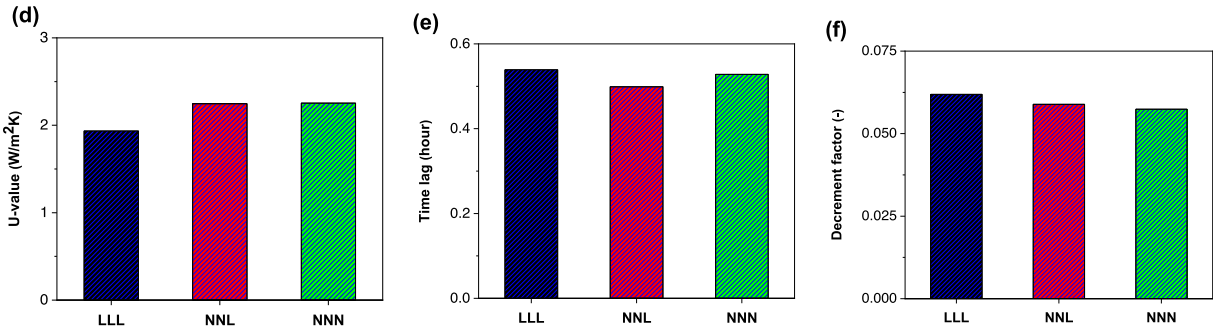

Fig. 7. Thermal properties of tested panels: (a) U-value, (b) time lag; and (c) decrement factor.

Table 5
Comparison of thermal dynamic properties obtained by different methods.

	U_0	h_{si}/U_0	t_{lag}^{EXP}	t_{lag}^{FD}	t_{lag}^{ISO}	f^{EXP}	f^{FD}	f^{ISO}	f_{corr}^{ISO}
	W/m^{2}K	(-)	(hr)	(hr)	(hr)	(-)	(-)	(-)	(-)
LLL	1.934	20.68	0.539	0.506	0.597	0.0619	0.0619	0.880	0.049
NNL	2.246	17.81	0.499	0.589	0.603	0.0589	0.0605	0.850	0.055
NNN	2.254	17.75	0.528	0.628	0.517	0.0574	0.0567	0.858	0.055

air temperature at the hot-side and cold-side boxes was used as the FD method's inputs; therefore, their values matched closely with each other. Overall, the time lag obtained through the ISO method also shows good agreement with the experimental values, whereas the decrement factor calculated by the ISO equation (f^{ISO}) indicates a significant discrepancy. For the time lag, the indoor sur-

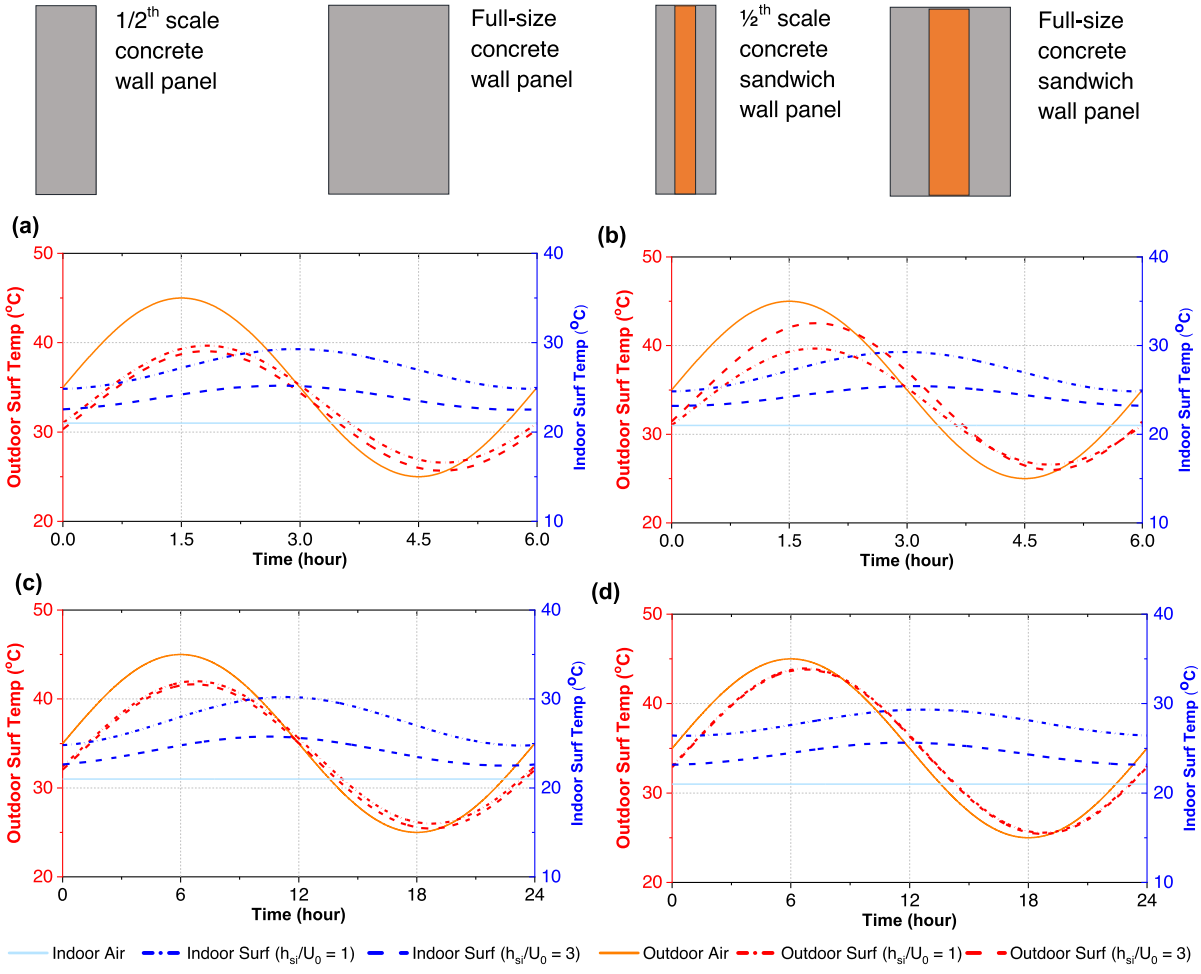

Fig. 8. Periodic temperature responses of concrete wall panels simulated by FD method: (a) ½ scale concrete wall panel; (b) ½ scale concrete sandwich wall panel; (c) full-size concrete wall panel; (d) full-size concrete sandwich wall panel.

face convection coefficient (h_{si}) has a negligible influence on the result obtained by the ISO method when it is large (see Equation (26) of *Section 2.3.1*). In the experiment study, 40.0 W/m^{2}K was used as the h_{si} to consider the effect of crossflow fan and potential thermal radiation from the alumina baffle and fin-heater. On the other hand, the decrement factor obtained by the ISO method depends on h_{si}/U_0 (see Equation (33)), which cannot be ignored when its value deviates from 1. Using h_{si}/U_0 as a correction coefficient, the corrected decrement factors of the ISO method (f^{ISO}_{corr}) were obtained and closely matched by the finite difference method.

4.3. Discussions

In the above sections, the feasibility of using the developed small-scale hot box was validated to measure the dynamic thermal properties (time lag and decrement factor) of the scaled-down specimen and the correspondence between the ISO method and finite difference method. In this section, we further validate the scaling relationship and the equivalence relationship between the ISO method and the finite difference method through different cases. The studies were conducted for the 1/3rd scale, the ½ scale, and full-size specimen of single layer concrete wall panel and concrete sandwich wall panel under various indoor surface convection conditions. The periods of the sinusoidal excitation are 2.667 h, 6 h, and 24 h, respectively, according to Equation (11).

As presented in *Section 2.3*, the equivalence of time lag and decrement factor between the ISO method and the finite difference method requires that the value of h_{si}/U_0 of the scaled-down specimen test equals its full-size counterpart (see Equation (30)). Since U_0 is proportionally related to the thickness (linear dimension scale) of an envelope assembly ($U_0^{SD} = nU_0^{FS}$) when the same materials are used to build the scaled-down model, and the indoor surface convection coefficient, h_{si}, is expressed as a function of surface air velocity [41]:

$$h_{si} = a + b v_{si} \tag{3}$$

where v_{si} is air velocity over the indoor surface; a and b are parameters related to the surface condition (i.e., roughness) and materials. Therefore, during the experiments on scaled specimens, h_{si} can be tuned by controlling the air velocity across the envelope surface to get close to the n folds of h_{si} of the full-size specimens. Under such circumstances, the time lag determined by the scaled-down experiments will be proportional to that of a full-size specimen (see Fig. 8 (a) and (c)). This also holds true for a multi-layer envelope assembly such as concrete sandwich panels (see Fig. 8 (b) and (d) and Table 6). In addition, it was observed that the increase of h_{in}/U_0 usually leads to the decrease of both time lag and decrement factor under the same outdoor conditions.

Table 6 lists the time lag and decrement factor obtained from FD simulations for both scaled and the corresponding full-scale wall panel specimens. It confirms that when the condition $(h_{si}/U_0)^{SD} = (h_{si}/U_0)^{FS}$ is met, a scaled-down experiment can equivalently represent a full-scale test. Since h_{si} can be adjusted by varying the air velocity across the test specimen's surface, it is feasible to conduct scale-down hotbox experiments to characterize both the static (steady-state) and dynamic thermal properties. It is worthwhile to mention that the value of f^{ISO}/f^{FD} equals to h_{si}/U_0 as discussed in *Section 4.2* for the corrected decrement factor of the ISO method.

Table 6
Validation of the equivalence between ISO method and FD method*

	Single Layer Concrete Wall Panel			Concrete Sandwich Wall Panel		
	Full-scale (6″-thick)	½th scale(3″-thick)	$^1/_3^{th}$ scale (2″-thick)	Full-scale(2″-2″-2″)	½th scale(1″-1″-1″)	$^1/_3^{th}$ scale($^2/_3$″- $^2/_3$″- $^2/_3$″)
	$(h_{si}/U_0)^{SD} = (h_{si}/U_0)^{FS} = 1$					
U_0 (W/m^{2}K)	2.78	5.55	8.27	0.66	1.33	1.98
t^{ISO}_{lag}(hr)	4.55	1.14	0.51	5.96	1.49	0.66
t^{FD}_{lag}(hr)	4.55	1.13	0.51	5.96	1.49	0.66
$t^{ISO}_{lag}/t^{FD}_{lag}$	1.00	1.00	1.00	1.00	1.00	1.00
f^{ISO}	0.34	0.34	0.34	0.16	0.16	0.16
f^{FD}	0.34	0.34	0.34	0.16	0.16	0.16
f^{ISO}/f^{FD}	1.00	1.00	1.00	1.00	1.00	1.00
	$(h_{si}/U_0)^{SD} = (h_{si}/U_0)^{FS} = 3$					
U_0 (W/m^{2}K)	2.78	5.55	8.27	0.66	1.33	1.98
t^{ISO}_{lag}(hr)	3.73	0.93	0.42	5.01	1.25	0.56
t^{FD}_{lag}(hr)	3.73	0.93	0.42	5.01	1.25	0.56
$t^{ISO}_{lag}/t^{FD}_{lag}$	1.00	1.00	1.00	1.00	1.00	1.00
f^{ISO}	0.60	0.60	0.60	0.40	0.40	0.40
f^{FD}	0.20	0.20	0.20	0.13	0.13	0.13
f^{ISO}/f^{FD}	3.00	3.00	3.00	3.00	3.00	3.00
$(h_{si}/U_0)^{SD} = (h_{si}/U_0)^{FS}$						
U_0 (W/m^{2}K)	2.78	5.55	8.27	0.66	1.33	1.98
h_{si} (W/m^{2}K)	4.00	8.00	12.00	4.00	8.00	12.00
t^{ISO}_{lag}(hr)	4.28	1.07	0.48	4.09	1.02	0.46
t^{FD}_{lag}(hr)	4.28	1.07	0.48	4.09	1.02	0.45
$t^{ISO}_{lag}/t^{FD}_{lag}$	1.00	1.00	1.00	1.00	1.00	1.00
f^{ISO}	0.43	0.43	0.43	0.61	0.61	0.61
f^{FD}	0.30	0.30	0.30	0.10	0.10	0.10
f^{ISO}/f^{FD}	1.45	1.45	1.45	6.00	6.00	6.00

* Concrete C1 and EPS were used as the concrete and insulation material, respectively.

5. Conclusions

This study evaluated the dynamic thermal performance of building envelope components (i.e., single or multi-layer wall panels) using small-scale calibrated hot box tests and scaled-down specimens. Small-scale hot box equipment was constructed and calibrated using a rigid foam panel with known R-value and applied to the tests of three scaled-down concrete sandwich wall panels. Moreover, scaling relationships for dynamic thermal properties of building envelope components between full-size and scaled-down specimens were established through analytical relationships validated by both experimental tests and finite difference (FD) simulation results. The following conclusions are drawn in this study:

- It is demonstrated that using a small-scale calibrated hot box and scaled-down specimen to evaluate the performance of building envelope elements is feasible. It has the merits of drastically lower experimental costs and experimentation time. The developed small-scale calibrated hot box equipment can be applied to both steady-state and transient heat transfer tests of building envelopes.
- The deducted scaling relationship for dynamic thermal properties of building envelope components between full-size and scaled-down specimens shows that the time lag is correlated by a coefficient of $1/n^2$. At the same time, the decrement factor does not change when an outdoor periodic excitation drives the scaled-down specimen with $1/n^2$ period of the full-size specimen. The indoor surface heat convection coefficient satisfies $h_{in}/U_0 = 1$. The h_{in} of the scaled-down specimen test can be tuned by controlling the air velocity across the envelope surface to get close to the n folds of h_{in} of the full-size specimens in a typical indoor condition.

A scaled-down specimen test is demonstrated as an effective and economical way to determining both the static (steady-state) and dynamic thermal properties of building envelope components as it reduces the time to $1/n^2$ of the full-size specimen test. At the same time, it still provides reliable indications of thermal performance. It should be noted that the scale-down hot box experiment should not be viewed as a replacement for the full-scale standard test.

Declaration of Competing Interest

The authors declare that they have no known competing financial interests or personal relationships that could have appeared to influence the work reported in this paper.

Acknowledgments

This research is partially sponsored by the U.S. National Science Foundation (NSF CMMI-1954517 and 1663302). The funding supports from NSF is greatly appreciated. The authors would like to thank Mr. Dominic Hanna for his assistance during the experimental tests. This manuscript has been authored in part by UT-Battelle, LLC, under contract DE-AC05-00OR22725 with the US Department of Energy (DOE). The US government retains and the publisher, by accepting the article for publication, acknowledges that the US government retains a nonexclusive, paid-up, irrevocable, worldwide license to publish or reproduce the published form of this manuscript, or allow others to do so, for US government purposes. DOE will provide public access to these results of federally sponsored research in accordance with the DOE Public Access Plan.

References

[1] T. Ahmad, D. Zhang, A critical review of comparative global historical energy consumption and future demand : The story told so far, Energy Reports 6 (2020) 1973–1991, https://doi.org/10.1016/j.egyr.2020.07.020.
[2] D. Ürge-vorsatz, L.F. Cabeza, S. Serrano, C. Barreneche, Heating and cooling energy trends and drivers in buildings, Renew Sustain Energy Rev 41 (2015) 85–98, https://doi.org/10.1016/j.rser.2014.08.039.
[3] US Department of Energy. Windows and Building Envelope Research and Developement: Roadmap for Emerging Technologies. 2014.
[4] P. Ma, L.S. Wang, N. Guo, Energy storage and heat extraction - From thermally activated building systems (TABS) to thermally homeostatic buildings, Renew Sustain Energy Rev 45 (2015) 677–685, https://doi.org/10.1016/j.rser.2015.02.017.
[5] L.-S. Wang, P. Ma, E. Hu, D. Giza-Sisson, G. Mueller, N. Guo, A study of building envelope and thermal mass requirements for achieving thermal autonomy in an office building, Energy Build 78 (2014) 79–88, https://doi.org/10.1016/j.enbuild.2014.04.015.
[6] D. Mazzeo, G. Oliveti, N. Arcuri, Influence of internal and external boundary conditions on the decrement factor and time lag heat flux of building walls in steady periodic regime, Appl Energy 164 (2016) 509–531, https://doi.org/10.1016/j.apenergy.2015.11.076.
[7] F. Stazi, C. Bonfigli, E. Tomassoni, C. Di Perna, P. Munafò, The effect of high thermal insulation on high thermal mass: Is the dynamic behaviour of traditional envelopes in Mediterranean climates still possible?, Energy Build 88 (2015) 367–383, https://doiorg/10.1016/j.enbuild.2014.11.056.
[8] C.E.N. En, ISO 13786:2007., Thermal performance of building components - Dynamic thermal characteristics -, Calculation methods. (2007).
[9] A. Gasparella, G. Pernigotto, M. Baratieri, P. Baggio, Thermal dynamic transfer properties of the opaque envelope: Analytical and numerical tools for the assessment of the response to summer outdoor conditions, Energy Build 43 (2011) 2509–2517, https://doi.org/10.1016/j.enbuild.2011.06.004.
[10] M. Rossi, V.M. Rocco, External walls design: The role of periodic thermal transmittance and internal areal heat capacity, Energy Build 68 (2014) 732–740, https://doi.org/10.1016/j.enbuild.2012.07.049.
[11] H. Asan, Numerical computation of time lags and decrement factors for different building materials, Build Envrionment 41 (2006) 615–620, https://doi.org/10.1016/j.buildenv.2005.02.020.
[12] S.A. Al-Sanea, M.F. Zedan, Improving thermal performance of building walls by optimizing insulation layer distribution and thickness for same thermal mass, Appl Energy 88 (2011) 3113–3124, https://doi.org/10.1016/j.apenergy.2011.02.036.
[13] S.A. Al-Sanea, M.F. Zedan, S.N. Al-Hussain, Effect of thermal mass on performance of insulated building walls and the concept of energy savings potential, Appl Energy 89 (2012) 430–442, https://doi.org/10.1016/j.apenergy.2011.08.009.
[14] M. Ozel, C. Ozel, Effects of wall orientation and thermal insulation on time lag and decrement factor. 9th Int, Conf. Heat Transf. Fluid Mech. Thermodyn., Malta (2012) 680–684.
[15] N.C. Balaji, M. Mani, B.V.V. Reddy, Dynamic thermal performance of conventional and alternative building wall envelopes, J Build Eng 21 (2019) 373–395, https://doi.org/10.1016/j.jobe.2018.11.002.
[16] F. Asdrubali, G. Baldinelli, Thermal transmittance measurements with the hot box method: Calibration, experimental procedures, and uncertainty analyses of three different approaches, Energy Build 43 (2011) 1618–1626, https://doi.org/10.1016/j.enbuild.2011.03.005.
[17] N. Soares, C. Martins, M. Gonçalves, P. Santos, L. Simões, J.J. Costa, Laboratory and in-situ non-destructive methods to evaluate the thermal transmittance and behavior of walls, windows, and construction elements with innovative materials: A review, Energy Build 182 (2019) 88–110, https://doi.org/10.1016/j.enbuild.2018.10.021.
[18] W.C. Brown, D.G. Stephenson, A guarded hot box procedure for determining the dynamic response of full-scale wall specimens - Part I, ASHRAE Trans 99 (1993) 632–642.
[19] W.C. Brown, D.G. Stephenson, Guarded hot box measurements of the dynamic heat transmission characteristics of seven wall specimens - Part II, ASHRAE Trans 99 (1993) 643–660.
[20] Koray Ulgen, Experimental and theoretical investigation of effects of wall's thermophysical properties on time lag and decrement factor, Energy Build 34 (3) (2002) 273–278.
[21] J.M. Sala, A. Urresti, K. Martin, I. Flores, A. Apaolaza, Static and dynamic thermal characterisation of a hollow brick wall: Tests and numerical analysis, Energy Build 40 (2008) 1513–1520, https://doi.org/10.1016/j.enbuild.2008.02.011.
[22] K. Martin, A. Campos-celador, C. Escudero, I. Gómez, J.M. Sala, Analysis of a thermal bridge in a guarded hot box testing facility, Energy Build 50 (2012) 139–149, https://doi.org/10.1016/j.enbuild.2012.03.028.
[23] K. Martin, I. Flores, C. Escudero, A. Apaolaza, J.M. Sala, Methodology for the calculation of response factors through experimental tests and validation with simulation, Energy Build 42 (2010) 461–467, https://doi.org/10.1016/j.enbuild.2009.10.015.
[24] N. Bishara, G. Pernigotto, A. Prada, M. Baratieri, A. Gasparella, Experimental determination of the building envelope's dynamic thermal characteristics in consideration of hygrothermal modelling – Assessment of methods and sources of uncertainty, Energy Build 236 (2021), https://doi.org/10.1016/j.enbuild.2021.110798 110798.

[25] A. Barbaresi, M. Bovo, E. Santolini, L. Barbaresi, D. Torreggiani, P. Tassinari, Development of a low-cost movable hot box for a preliminary definition of the thermal conductance of building envelopes, Build Environ 180 (2020), https://doi.org/10.1016/j.buildenv.2020.107034 107034.
[26] E. Kossecka, J. Kosny, Hot-Box Testing of Building Envelope Assemblies — A Simplified Procedure for Estimation of Minimum Time of the Test, J Test Eval 36 (2007) 242–249.
[27] Seitz S, Macdougall C. Design of an Affordable Hot Box Testing Apparatus. Proc. 16th NOCMAT, Winnipeg, Canada: 2015.
[28] C. Buratti, E. Belloni, L. Lunghi, M. Barbanera, Thermal Conductivity Measurements by Means of a New 'Small Hot-Box' Apparatus: Manufacturing, Calibration and Preliminary Experimental Tests, Int J Thermophys 37 (2016) 1–23, https://doi.org/10.1007/s10765-016-2052-2.
[29] Modi P, Bushehri R, Georgantopoulou C. Advances in Building Energy Research Design and development of a mini scale hot box for thermal efficiency evaluation of an insulation building block prototype used in Bahrain. Adv Build Energy Res 2016;2549. 10.1080/17512549.2016.1161545.
[30] O'Leary TP, Duffy A. The Design, Construction and Commissioning of a Small Scale Dynamic Calibrated Hot Box (CHB). 7th Int. Build. Physcis Conf., Syracuse, New York, USA: 2018.
[31] X. Zhao, S.A. Mofid, M.R. Al, G.W. Saxe, B. Petter, Reduced-scale hot box method for thermal characterization of window insulation materials, Appl Therm Eng 160 (2019), https://doi.org/10.1016/j.applthermaleng.2019.114026 114026.
[32] Louis A. Pipes, Matrix analysis of heat transfer problems, J Franklin Inst 263 (3) (1957) 195–206.
[33] M.G. Davies, The Thermal Response of an Enclosure to Periodic Excitation: The CIBSE Approach, Build Environ 29 (2) (1994) 217–235.
[34] S.A. Al-Sanea, M.F. Zedan, Heat Transfer Characteristics and optimum insulation thickness for cavity walls, J Therm Environ Build Sci 26 (2003) 285–307, https://doi.org/10.1177/109719603027973.
[35] C.J. Schumacher, D.G. Ober, J.F. Straube, A.P. Grin, Development of a New Hot Box Apparatus to Measure Building Enclosure Thermal Performance, ASHRAE Therm. Perform. Exter. Envel. Whole Build. XII Int. Conf. (2013) 1–19.
[36] ISO 22007-2. Plastics - Determination of thermal conductivity and thermal diffusivity - Part 2: Transient plan heat source (hot disc) method 2015.
[37] ASTM C1363. Standard Test Method for Thermal Performance of Building Materials and Envelope Assemblies by Means of a Hot Box Apparatus. 2018. 10.1520/C1363-11.2.
[38] R.J. Onega, P.J. Burns, Thermal Flanking Loss Calculations for the National Bureau of, Standards Calibrated Hot Box. (1985).
[39] H. Zhou, A.L. Brooks, Thermal and mechanical properties of structural lightweight concrete containing lightweight aggregates and fly-ash cenospheres, Constr Build Mater 198 (2019) 512–526, https://doi.org/10.1016/j.conbuildmat.2018.11.074.
[40] S.E. Gustafsson, Transient diffusivity plane source techniques for thermal conductivity measurements of solid materials and thermal, Rev Sci Instrum 62 (1991) 797–804.
[41] M. Mirsadeghi, D. Cóstola, B. Blocken, J.L.M. Hensen, Review of external convective heat transfer coefficient models in building energy simulation programs: Implementation and uncertainty, Appl Therm Eng 56 (2013) 134–151, https://doi.org/10.1016/j.applthermaleng.2013.03.003.